BOLETÍN
DE
CIENCIAS DE LA TIERRA

https://revistas.unal.edu.co/index.php/rbct

Análisis y comparación de las transformadas de Fourier y Wavelet: aplicación para el estudio de parámetros de la fuente sísmica del Terremoto de Arequipa del 2001

Marilyn Katia Paredes-Huanca & Edgard Gonzales-Zenteno

Universidad Nacional de San Agustín de Arequipa, Perú. mparedeshua@unsa.edu.pe, hgonzalesz@unsa.edu.pe

Received: 20 febrero 2025. Received in revised form: 31 de julio de 2025. Accepted: 1 agosto 2025

Resumen

Este estudio se centra en la caracterización del terremoto de Arequipa del 23 de junio de 2001, aplicando conjuntamente la Transformada de Fourier (FFT) y la Transformada Wavelet (WT) para estimar los parámetros de fuente y la energía radiada, con el objetivo de mejorar la gestión del riesgo sísmico en el sur de Perú. Los resultados de FFT mostraron momentos sísmicos entre 3.55×10^{16} y 1.41×10^{18} N·m, caídas de estrés entre 0.46 y 3.99 MPa, y radios de fractura de 0.61 a 1.94 km. La WT permitió estimar frecuencias dominantes entre 0.18–0.24 Hz, energía radiada entre 24.52 y 32.19 J, y duraciones de ruptura entre 40.02 y 105.98 s. El uso combinado de FFT y WT permitió una caracterización más detallada del terremoto de 2001. La FFT resultó eficaz para el análisis espectral de los parámetros de fuente, mientras que la WT proporcionó estimaciones precisas de la energía radiada y la duración de la ruptura, factores clave para mejorar la evaluación del riesgo sísmico en la región.

Palabras clave: Transformada de Fourier (FFT); Transformada Wavelet (WT); energía radiada; parámetros fuente; terremoto de Arequipa.

Analysis and comparison of Fourier and Wavelet transforms: application to the study of seismic source parameters of the 2001 Arequipa Earthquake

Abstract

This study focuses on the characterization of the June 23, 2001, Arequipa earthquake by applying the Fourier Transform (FFT) and Wavelet Transform (WT) together to estimate source parameters and radiated energy, aiming to improve seismic risk management in southern Peru. FFT results showed seismic moments ranging from 3.55×10^{16} to 1.41×10^{18} N·m, stress drops between 0.46 and 3.99 MPa, and fracture radii from 0.61 to 1.94 km. WT enabled the estimation of dominant frequencies between 0.18–0.24 Hz, radiated energy ranging from 24.52 to 32.19 J, and rupture durations from 40.02 to 105.98 s. The combined use of FFT and WT allowed for a more detailed characterization of the 2001 Arequipa earthquake. FFT proved effective for spectral analysis of source parameters, while WT provided accurate estimates of radiated energy and rupture duration—key factors for enhancing seismic risk assessment in the region.

Keywords: Fourier Transform (FFT); Wavelet Transform (WT); radiated energy; source parameters; Arequipa earthquake.

1. Introduction

The characterization of seismic signals using spectral and time-frequency analysis techniques is essential for understanding earthquake rupture dynamics and improving early warning and hazard mitigation models. Due to their inherently non-stationary nature, seismic signals pose significant challenges to classical techniques such as the Fourier Transform (FT), which, although effective in identifying dominant frequencies, loses information about the temporal evolution of the spectral content [1]

As an alternative, the Wavelet Transform (WT)—in both its continuous and discrete forms—offers a multiresolution representation in the time-frequency domain, enabling the analysis of signals with dynamic variations and abrupt transitions [2]. Its application has proven effective in studies

How to cite: Paredes-Huanca, M.K., and Gonzales-Zenteno, E., (2025). Analysis and comparison of Fourier and Wavelet Transforms: application to the study of seismic source parameters of the 2001 Arequipa Earthquake.. BOLETÍN DE CIENCIAS DE LA TIERRA. 58, pp. 41-50. DOI:https://doi.org/10.15446/rbct.n58.118962

such as the 2015 Kathmandu Valley earthquake, where the temporal distribution of seismic energy was evaluated [3], and in regional-scale source parameter estimation [4].

In various regions worldwide, FT has been employed to estimate seismic source parameters such as seismic moment, corner frequency, and radiated energy. For example, in Cuba [5], South Africa [6], and Colombia [7], these methods have contributed to regional seismic characterization. In California, [8] used WT and the Brune model to evaluate energy release across events of varying magnitude, while [9] established empirical relationships between seismic moment and stress drop that remain foundational in modern seismology.

In the Peruvian context, [10] applied FT and the Brune model to the aftershocks of the 2001 Arequipa earthquake, revealing patterns of rupture and energy release. Similarly, [11] used FT to estimate source parameters from the aftershocks of the 2018 Lomas earthquake (Mw 7.1), assessing interactions between the mainshock and its aftershocks.

Despite these advances, an important gap remains: integrated approaches that combine spectral (FT) and time-frequency (WT) techniques are still scarce, particularly for complex events such as the 2001 Arequipa earthquake. This earthquake, with a magnitude of Mw 8.4, prolonged duration, multiple moment release pulses, and unilateral rupture propagation, represents an ideal case for applying and comparing both techniques jointly.

This study proposes the simultaneous application of FT and WT to seismic records from the 2001 Arequipa earthquake and its ten main aftershocks, to estimate source parameters such as seismic moment, stress drop, fracture radius, and radiated energy. By comparing the results from both transforms, the study seeks to demonstrate how the integration of these approaches enables a more complete and dynamic characterization of the seismic source, thereby enhancing seismic hazard assessment capabilities in southern Peru.

1.1 Study area

The study area is located in southern Peru, spanning from 15.6° to 18.2° south latitude, and from 68.7° to 76.2° west longitude. This region was affected by the 2001 earthquake, which had 134 aftershocks distributed southeastward, suggesting that the rupture propagated in that direction [12]. Fig. 1 illustrates the location of the study area and the distribution of aftershocks according to their magnitude. Blue circles correspond to aftershocks with Mw between 5 and 5.5, green circles from 5.5 to 6.5, and red circles from 6.5 to 7.5

The main Arequipa 2001 earthquake is represented by a yellow star, while the rupture zone is marked with a green rectangle.

The 2001 earthquake in southern Peru caused numerous fatalities and severe damage in Tacna, Arequipa, Ayacucho, and Moquegua, as well as in Arica and Iquique (Chile), with an intensity of VII-VIII on the Modified Mercalli scale [13]. The aftershock analysis identified a rupture area of 370 x 150 km², with propagation towards the southeast [14]. More than 80 localities were affected, with 217,400 people impacted and 17,580 houses destroyed [15]. Key seismic source parameters were determined through advanced studies, as reflected in Table 1, while Fig. 2 illustrates its focal mechanism and intensities.

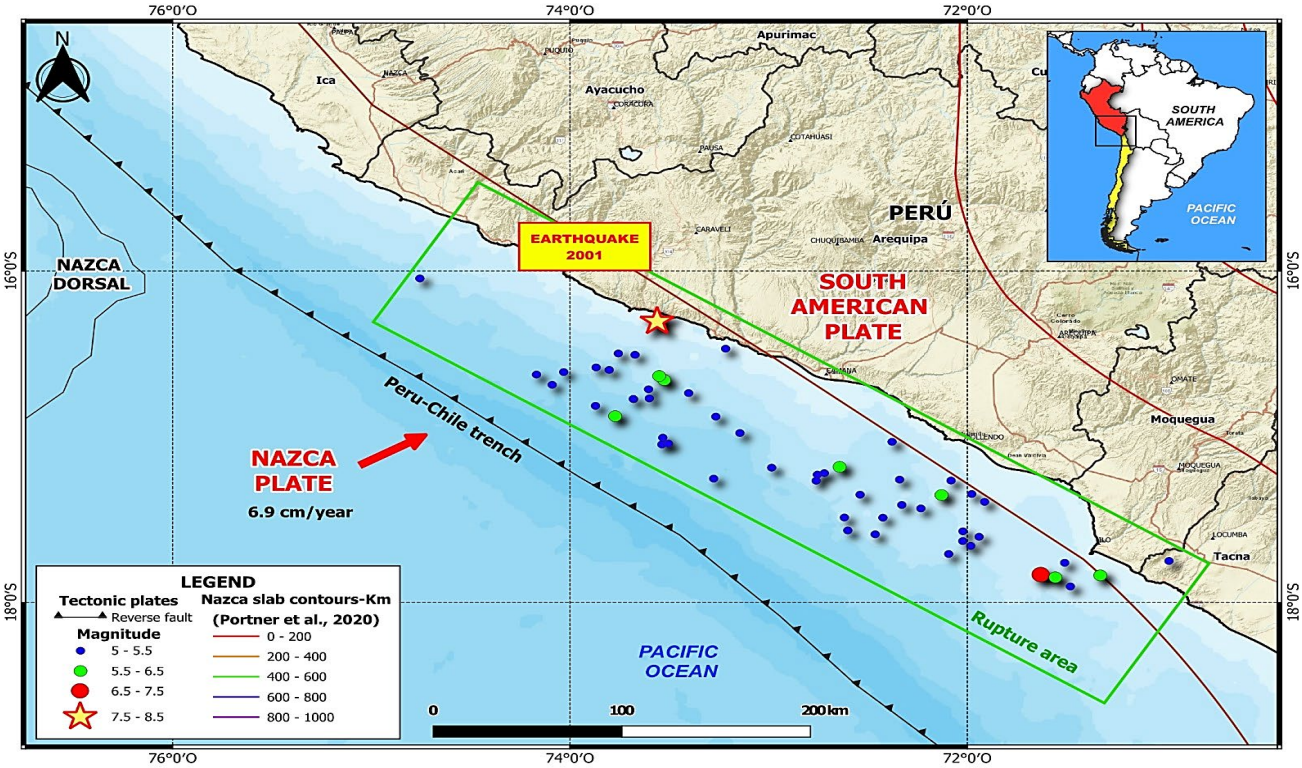

Figure 1. Geographic distribution of the study area, 2001 Arequipa earthquake epicenter, and spatial pattern of aftershocks by magnitude
Source: Adapted from Tavera, H. and Antayhua, 2022.

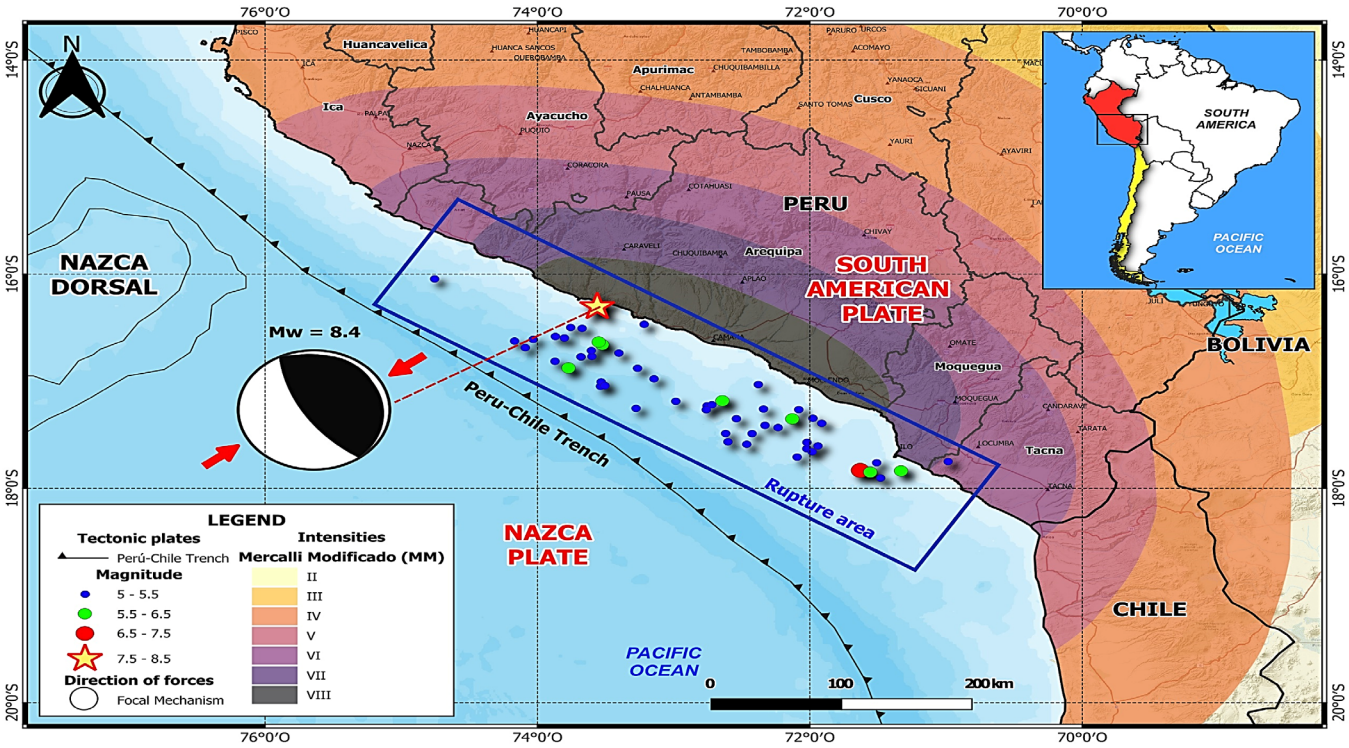

Figure 2. Focal mechanism and tectonic context of the 2001 Arequipa earthquake (Mw 8.4). The beach ball symbol illustrates a reverse fault mechanism. Red arrows indicate compressive forces from the Nazca Plate subducting beneath the South American Plate at ~6.9 cm/year. The rupture zone, aftershock distribution (colored by magnitude), and Modified Mercalli intensities across southern Peru are also depicted, highlighting the regional seismic impact
Source: Adapted from Tavera et al., 2020.

Table 1.
Source and impact parameters of the 2001 Arequipa earthquake (Mw 8.4).

Parameter	Value/Description
Date and time	June 23, 2001, at 15:33 (20:33 UTC)
Magnitude	8.4 Mw (Moment Magnitude Scale)
Epicenter	16.265°S, 73.641°W; 120km southwest
Focal Depth	33 km depth
Tsunami	Camaná, Peru
Duration	Between 60 and 120 seconds
Released Energy	Equivalent to 32 megatons of TNT
Focal Mechanism	Reverse Fault (Thrust Fault)
Strike	Approximately 308°
Dip	Around 20°
Rake	Around 72° (compressional movement)

Source: Adapted from Tavera, H. and Antayhua, 2022.

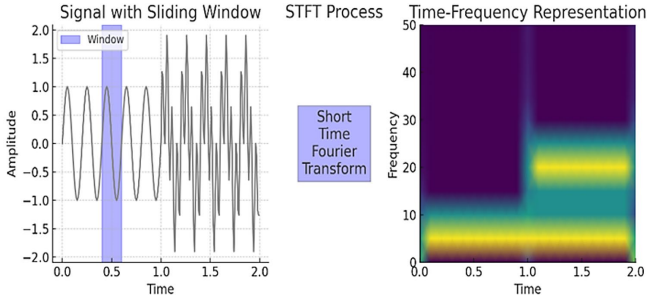

Figure 3. Schematic representation of the STFT for time-frequency analysis of seismic signals
Source: The authors

2. Theoretical framework

2.1 Fourier Transform (FFT)

The FFT is essential in seismology for analyzing seismic signals, decomposing them into their frequency components, and facilitating the interpretation of seismic phenomena [9]. The Fourier Series allows the representation of any periodic function as an infinite sum of sine and cosine functions at different frequencies. The coefficients a_k and b_k indicate the contribution of each frequency in the function [17].

$$x(t) = \frac{a_0}{2} + \sum_{k=1}^{\infty} \left(a_k cos(k\omega_0 t) + b_k sen(k\omega_0 t) \right) \qquad (1)$$

The Short-Time Fourier Transform (STFT) is essential for analyzing non-stationary signals, as it segments the signal into time windows to track changes in its frequency content [1]. The STFT enables a time-frequency analysis, where each window reveals the spectral distribution at that moment [18]. The result is a time-frequency graph, where the horizontal axis represents time and the vertical axis represents frequency, showing how frequencies evolve (Fig. 3).

2.2 Wavelet Transform (WT)

Unlike Fourier, the WT uses a mother wavelet, an oscillatory function localized in time and frequency, allowing the decomposition of signals into scaled and translated

Table 2.
Analysis and Comparison of Fourier Transform and Wavelet Transform - Seismology

Characteristic	Fourier Transform (FFT)	Wavelet Transform (WT)
Domain	Frequency	Time-Frequency
Transient Signal Analysis	Not suitable for transient signal analysis	Suitable for transient signal analysis
Temporal Resolution	Poor	Good temporal resolution
Frequency Resolution	High frequency resolution	Variable frequency resolution
High applicability in seismic signal analysis	Good for periodic or stationary signals	Ideal for non-stationary seismic signals, such as earthquakes and transient events
Fixed vs Variable Window	Fixed Window vs Variable Window	Use a variable window, shorter for high frequencies and longer for low frequencies.
Ability to detect local events.	It is not effective in detecting seismic events.	Very effective for detecting local events, such as earthquakes or seismic ruptures.
Computational Complexity	Less computationally expensive.	More computationally expensive.
Use in frequency identification	Good for identifying dominant frequencies throughout the signal.	Can identify frequencies that vary over time, useful for non-constant seismic events.
Common Applications in Seismology	Detection of fundamental frequency of seismic signals	Earthquake analysis and non-stationary signals. Identification of seismic phases.

Source: Adapted from Bessissi et al., 2009.

components [17]. This method enables concurrent analysis in both time and frequency domains, facilitating the identification of trends and oscillations [19]. CWT spectra, amplitudes are represented through a chromatic scale where warm colors (reds/oranges) indicate higher energy magnitudes, while cool colors (blues/greens) correspond to lower amplitudes [2]. Eq. (2) defines a scaled and translated wavelet used in the Continuous Wavelet Transform (CWT) [20].

$$\Psi^*_{a,b}(t) = |a|^{-\frac{1}{2}}\Psi^*\left[\frac{t-b}{a}\right] a, b \in R \; y \; a \neq 0 \qquad (2)$$

Fig. 4 shows the process of the WT, a technique for analyzing signals in the time and scale domains [21]. The input signal represents a vibration that varies over time [22]. During the Wavelet Transform process, the signal is decomposed into different scales to identify its frequency content over time [23]. The analysis reveals that large scales correspond to low frequencies, while small scales capture high frequencies, enabling more detailed resolution than the Fourier Transform [2]. In Table 2, a comparison of FFT and WT in terms of seismology is presented.

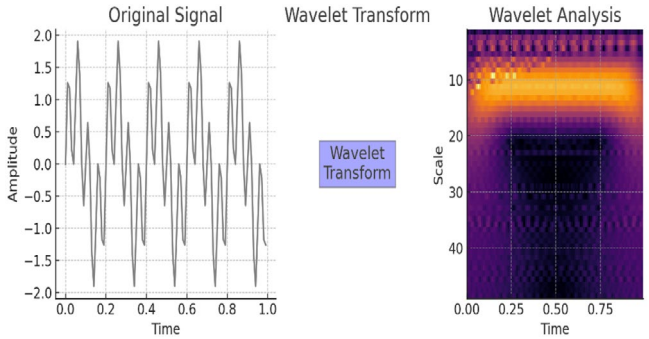

Figure 4. Conceptual diagram of the WT for multiscale time-frequency analysis of seismic signals
Source: The authors.

3 Data and methodology

3.1. Database download

The data were obtained from the IRIS seismic network, specifically from the Ñaña station (NNA), located at latitude -11.988° and longitude -76.842°, selected for its proximity to the earthquake epicenter.

Fig. 5 shows the flowchart of the process followed in this research. The diagram outlines a detailed and structured approach to analyzing seismic signals using two complementary techniques: FFT and WT. The results from both methods were used to determine fundamental parameters about the seismic source, allowing for a better understanding of the nature of earthquakes and their aftershocks. Once the data (10 aftershocks) were downloaded, two main programs were used to process the data.

The aftershock data were selected between June 23 and July 1, 2001, with magnitudes ranging from 5 to 10, and depths from 0 to 75 km. The selection of aftershocks was guided by the need to ensure waveform quality and consistency in depth and magnitude for reliable waveform analysis. Events with magnitudes ≥5.0 and depths ≤75 km were chosen to maintain a homogeneous dataset suitable for spectral and time-frequency analysis. This threshold also ensures that selected events generate records with a sufficient signal-to-noise ratio, essential for accurate estimation of source parameters. Although other events of lower magnitude exist, they were excluded due to limitations in data quality or lack of clear waveform characteristics. Table 3 shows the database of the 10 aftershocks, with their main characteristics (Date, time, latitude, longitude, depth, magnitude type, and location).

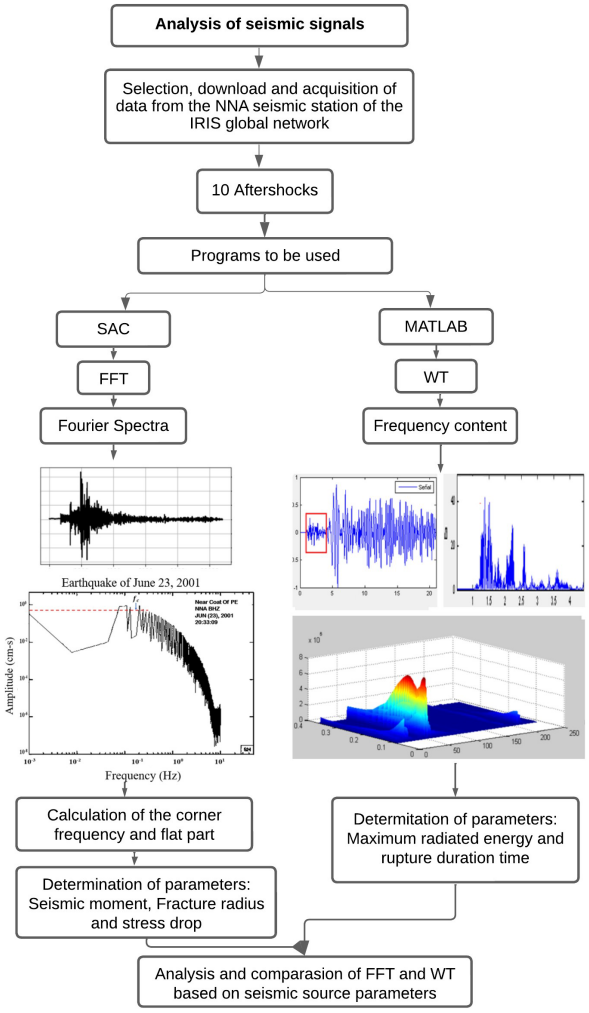

Figure 5. Flowchart of the methodological framework for seismic signal analysis using FFT and WT
Source: The authors

3.2. Determination of seismic source parameters with FFT

The Seismic Analysis Code (SAC) software is a widely used tool in seismology for the management and analysis of seismic data in time series [25]. It allows the application of FFT to calculate the spectrum of a signal and uses high-pass, low-pass, and band-pass filters to remove noise and enhance seismic detection [26].

SAC is essential for determining seismic source parameters such as Mo, source radius, corner frequency fc, and stress drop ($\Delta\sigma$), allowing the analysis of fault dynamics and potential damage.

For seismic signal processing, high-pass, low-pass, and band-pass filters were applied using SAC software to eliminate noise and enhance spectral detection. Signals were corrected to physical units suitable for calculating parameters such as Mo and $\Delta\sigma$. In the Wavelet analysis, signals were bandpass filtered between 2 and 4 Hz, amplitudes were squared, absolute values were taken, then smoothed, and normalized to unity.

The fc is related to the rupture size and earthquake duration, being lower in high-magnitude events and higher in smaller ones [27]. The flat part of the spectrum (Ω_0) is found at low frequencies, where the amplitude is constant, indicating a uniform distribution of energy [28] (Fig. 6).

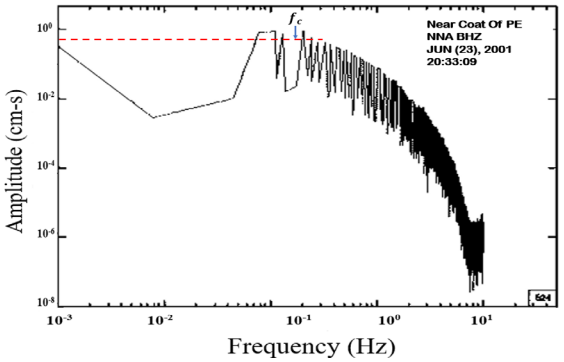

Figure. 6. Fourier spectrum, calculating the corner frequency fc and the flat part Ω_0, of the 2001 Arequipa earthquake.
Source: The authors

Table 3.
Seismological parameters of the 2001 Arequipa earthquake and its ten selected aftershocks

Item	Date	Time	Latitude	Longitude	Depth	Mag.	Mag	Location
Earthquake	23/06/2001	20:33:09	-16.303	-73.561	33.0	8.4	Mw	Coast of Peru
Aftershocks 1	23/06/2001	21:27:35	-17.181	-72.642	33.0	6.1	Mw	Coast of Peru
Aftershocks 2	23/06/2001	23:09:57	-16.657	-73.525	10.0	5.9	Mw	Coast of Peru
Aftershocks 3	25/06/2001	3:48:58	-16.044	-74.755	33.0	5.3	Mw	Coast of Peru
Aftershocks 4	25/06/2001	6:38:48	-16.875	-73.772	38.0	5.7	Mw	Coast of Peru
Aftershocks 5	26/06/2001	4:18:32	-17.831	-71.63	33.0	6.7	Mw	Coast of Peru
Aftershocks 6	26/06/2001	8:47:09	-16.624	-74.168	33.0	5.4	Mw	Coast of Peru
Aftershocks 7	27/06/2001	0:21:06	-17.903	-71.480	33.0	5.4	Mw	Coast of Peru
Aftershocks 8	28/06/2001	21:35:24	-17.588	-72.463	33.0	5.3	Mw	Coast of Peru
Aftershocks 9	30/06/2001	8:57:19	-17.707	-72.093	33.0	5.3	Mw	Coast of Peru
Aftershocks 10	01/07/2001	11:06:30	-17.186	-72.984	33.0	5.4	Mw	Coast of Peru

Source: The authors

3.2.1. Calculation of seismic moment (Mo)

The *Mo* was calculated using the flat part of the displacement spectrum (Ωo), following the classical formulation proposed by [28. This equation relates the observed spectral amplitude to source parameters, accounting for density, wave velocity, epicentral distance, and radiation pattern, as expressed in Eq. (3):

$$M_o = \frac{4\pi\rho v^3}{2\psi_0} R\Omega_0 \quad (3)$$

Ω_0 = Flat part, calculated from the spectrum
M_o = Seismic moment.
ρ= Density of the medium; 2.8 gr/cm3
R=Epicentral distance
v = P-wave velocity; 5 Km/seg
ψ_0= Radiation pattern, assumed as 0.4 based on a double-couple source model with isotropic take-off angle distribution [28] (Brune, 1970).

3.2.2. Calculation of the fracture radius

The fracture radius is a crucial parameter that defines the spatial extent of the rupture zone during an earthquake. Its estimation helps improve understanding of the fault's geometry and the energy release scale. Based on the fc obtained from spectral analysis, the fracture radius (Eq. 4) can be calculated using standard formulations derived from source theory models.

$$r_0 = \frac{2.34\alpha}{2\pi f_c} \quad (4)$$

α = represents the speed of the P-wave

3.2.3. Calculation of stress drop (Δσ)

Stress drop indicates the difference in shear stress on a fault before and after rupture and is directly linked to the energy released during an earthquake. It is a key parameter for understanding rupture behavior and seismic efficiency. Using the previously estimated Mo and fracture radius, Δσ (Eq. 5) can be calculated using classical source scaling relationships.

$$\Delta\sigma = 0.44(M_o/r^3) \quad (5)$$

3.3. Determination of seismic source parameters with WT

MATLAB is a key tool in technical scientific programming, enabling seismic signal analysis through digital processing, including the interpretation of phases, amplitude, and polarity [29]. Additionally, it facilitates the use of the Continuous Wavelet Transform (CWT) to represent non-stationary signals in the time-frequency domain [30].

The use of MATLAB and the Wavelet Transform allows for the analysis of non-stationary seismic signals, decomposing them into different frequency and time scales to characterize the dynamics of the seismic source [31]. The seismic signal shows energy variations over time, with higher energy at low frequencies (surface waves) in the first minutes, which decreases over time. In Fig. 7, high scales correspond to low frequencies, associated with surface waves, while low scales represent high frequencies of P or S waves. High intensity peaks indicate energy release, and the decrease towards the end reflects the reduction in seismic activity.

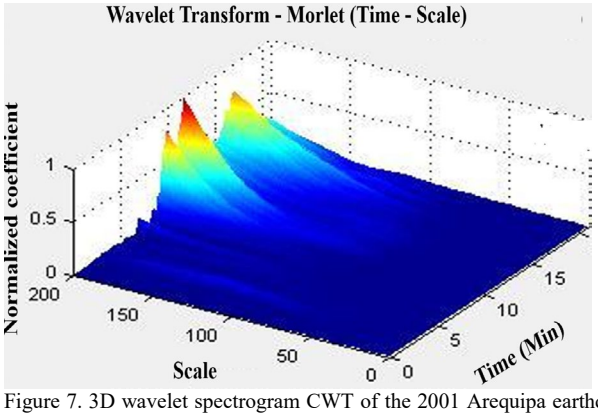

Figure 7. 3D wavelet spectrogram CWT of the 2001 Arequipa earthquake, generated in MATLAB
Source: The authors.

3.3.1. Calculation of rupture time

The rupture time was estimated following the methodologies of [32]. The vertical BHZ component was filtered between 2–4 Hz, squared, and normalized to enhance signal clarity. Rupture duration was then measured from the P-wave onset to the point where the amplitude decayed to 20% of its maximum, providing reliable results without the need for instrumental response correction.

The seismic record used for this analysis corresponds to a vertical BHZ component, with a velocity equivalent to that of a broadband station, allowing for a detailed study of the waveforms [33] (Fig.8a). To enhance the clarity of the signal, a bandpass filter is applied to the record, restricting frequencies to a range of 2 to 4 Hz, which effectively isolates the relevant seismic frequencies while minimizing noise interference (Fig. 8b).

Once the filtered signal is obtained, its amplitude values are squared, making them proportional to the seismic energy radiation. Additionally, to facilitate further processing, the absolute values of the amplitudes are taken, smoothed, and normalized to unity, ensuring a consistent comparison across different signals [34]. This transformation allows a better understanding of the energy distribution and variations within the seismic event.

In terms of signal decay analysis, the duration of the pause is measured from the initial arrival of the P-wave until the amplitude reduces to 20% of its maximum value, providing insights into the dissipation of seismic energy over

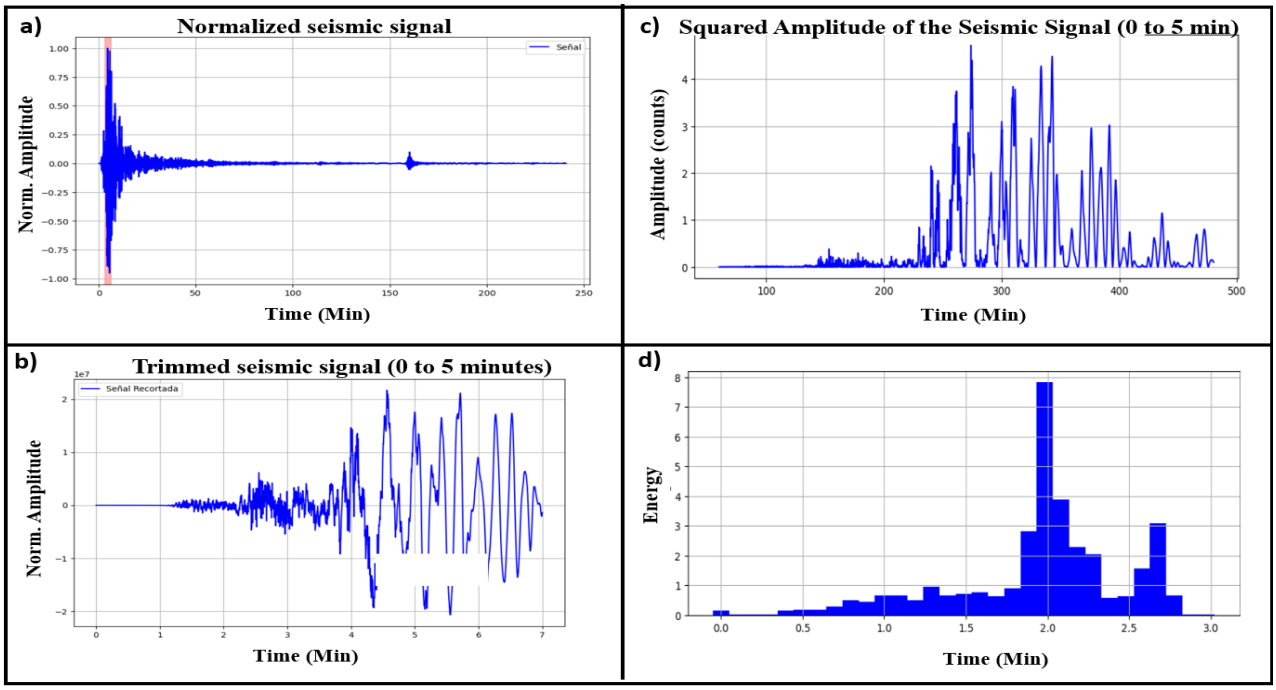

Figure. 8. (a) Vertical component seismic signal of the Arequipa Earthquake of 2001, (b) Normalized seismic signal (P-wave), (c) Calculation of rupture duration, (d) Calculation of maximum radiated energy MaxEa (J)
Source: The authors.

time. This approach highlights the gradual attenuation of the seismic waves and their energy release patterns [35].

It is also crucial to emphasize that, since the analysis focuses only on the temporal component of the seismic signal, adjusting the instrumental response is not required. This simplifies the workflow while maintaining the integrity of the data, ensuring that the results remain reliable and representative of the actual seismic phenomenon under investigation. Since the analysis relies on the signal's temporal evolution rather than absolute amplitude, instrumental correction is unnecessary. The waveform shape remains intact, preserving data integrity and ensuring reliable, representative results of the seismic event (Fig. 8c).

3.3.2. Calculation of Maximum Radiated Energy (MaxEa)

The maximum radiated energy (MaxEa) is obtained by summing the amplitudes from the wavelet spectrogram in a specific frequency band (2–4 Hz in this study), following the energy integration method [36]. The temporal distribution of seismic energy, which is crucial for estimating Mo and magnitude, shows a progressive decrease, indicating rapid dissipation of waves in events with high attenuation. The radiated energy can be obtained by calculating the sum of the amplitudes of the WT spectrogram in a specific frequency band (Fig. 8d).

4 Results and discussion

The Fourier spectra were plotted for the 10 aftershocks of the Arequipa earthquake of 2001, determining the flat part (Ω_0) and the fc, essential for calculating the seismic source parameters. The Wavelet analysis of the 10 aftershocks from the 2001 Arequipa earthquake was carried out using MATLAB, where the methodology was fully implemented.

4.1. Comparison of the parameters of the Arequipa 2001 earthquake and its aftershocks

Table 4 presents the main source parameters: Mo, R, and Δσ estimated using FFT; and Fc, MaxEa, and Tr obtained using WT. These values provide complementary information on the event's size, energy release, and rupture dynamics.

Table 5 summarizes the seismic source parameters obtained through FFT and WT transforms, comparing the mainshock (Mw 8.4) and its aftershocks (Mw 5.3–6.7), including M_0, fracture radius, stress drop (Δσ), radiated energy (MaxEa), and rupture durations.

Table 4.
Seismic source parameters and corresponding estimation methods using FFT and WT

Parameter	Unit	Method
Seismic Moment (Mo)	N·m	FFT
Fracture Radius	km	FFT
Stress Drop (Δσ)	MPa	FFT
Frequency Content	Hz	WT
Maximum Radiated Energy (MaxEa)	J	WT
Rupture Duration	s	WT

Source: The authors.

Table 5.
Seismic source parameters derived from FFT (M_0, fracture radius, $\Delta\sigma$) and WT (dominant frequency, MaxEa, duration) for the 2001 Arequipa mainshock and aftershocks.

Ítem			FFT			WT		
	Depth (km)	Mw	Mo (N.m)	Radio (Km)	Δσ (Mpa)	Frec (Hz)	MaxEa (J)	Dur Rupt. (s)
Earthquake	33.0	8.4	1.58×10^{21}	3.15	38.08	0.30	40.80	146.12
Aftershock 1	33.0	6.1	3.55×10^{17}	1.82	2.88	0.18	29.22	95.18
Aftershock 2	10.0	5.9	1.12×10^{17}	1.71	1.83	0.20	28.27	82.00
Aftershock 3	33.0	5.3	3.55×10^{16}	0.73	0.57	0.19	24.52	40.02
Aftershock 4	38.0	5.7	8.91×10^{16}	1.36	1.79	0.24	26.82	70.18
Aftershock 5	33.0	6.7	1.41×10^{18}	1.94	3.99	0.19	32.19	105.98
Aftershock 6	33.0	5.4	4.47×10^{16}	1.11	1.48	0.19	25.21	54.21
Aftershock 7	33.0	5.4	4.47×10^{16}	1.13	1.46	0.18	25.78	59.58
Aftershock 8	33.0	5.3	3.55×10^{16}	0.61	0.64	0.19	24.69	43.93
Aftershock 9	33.0	5.3	3.55×10^{16}	0.76	0.46	0.18	24.78	45.08
Aftershock 10	33.0	5.4	4.47×10^{16}	1.12	1.58	0.19	25.99	50.89

Source: The authors

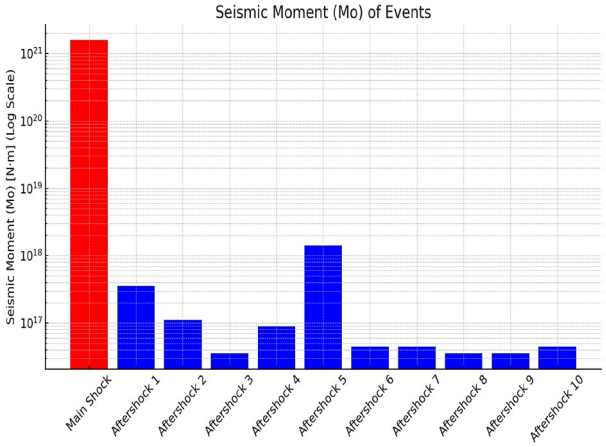

Figure. 9. Seismic Moment Values for the Arequipa Earthquake (Main Shock) and its Aftershocks.
Source: The authors

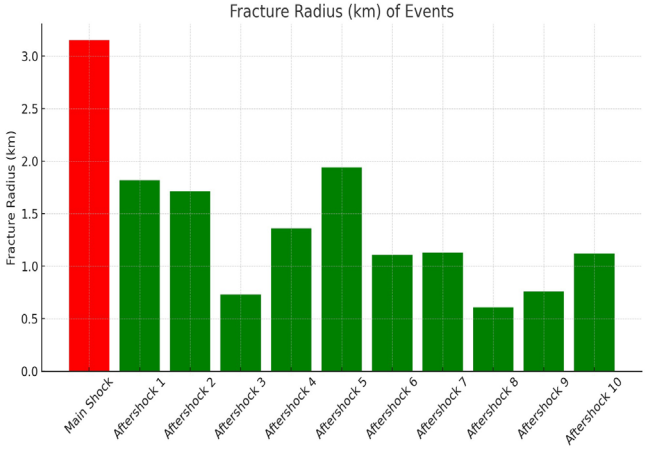

Figure. 10. Fracture Radius for the Arequipa Earthquake (Main Shock) and its Aftershocks
Source: The authors

4.2. Seismic Moment (Mo)

Fig. 9 illustrates the seismic moment (Mo) of the main shock and aftershocks using a logarithmic scale on the vertical axis to capture the wide range of values. The main shock, represented in red, exhibits a seismic moment of 1.58×10^{21} N·m. This reflects the immense amount of energy released during the primary rupture. In contrast, the aftershocks, shown in blue, have significantly lower moments, ranging from 3.55×10^{16} N·m to 1.41×10^{18} N·m. These events mainly contributed to the release of residual stresses and had a much smaller impact on the overall deformation. The use of a logarithmic scale emphasizes the contrast in energy between the main event and the subsequent seismic.

4.3. Fracture Radius

Fig. 10 presents the fracture radius (in kilometers) for each seismic event. The main shock, again in red, displays the largest fracture radius—3.15 km—indicating a much greater rupture area compared to the aftershocks, which are shown in green. The aftershocks generally range between 0.6 km and 2 km in radius. This graph clearly highlights the spatial extent of the main rupture compared to the more localized failures of the smaller seismic events. The use of contrasting colors once more helps differentiate the dominant main shock from the supporting seismic sequence.

Fig. 11 displays the log-log relationship between Mo (N·m) and fracture radius (r), with lines representing different values of stress drop ($\Delta\sigma$ = 0.1, 1, 10, and 100 MPa). The red star marks the mainshock, located above the 10 MPa line, while the aftershocks cluster near the same line, suggesting similar stress drop magnitudes. This graphical representation follows the scaling law $\Delta\sigma \propto M_0 / r^3$, allowing for visual interpretation of rupture mechanics.

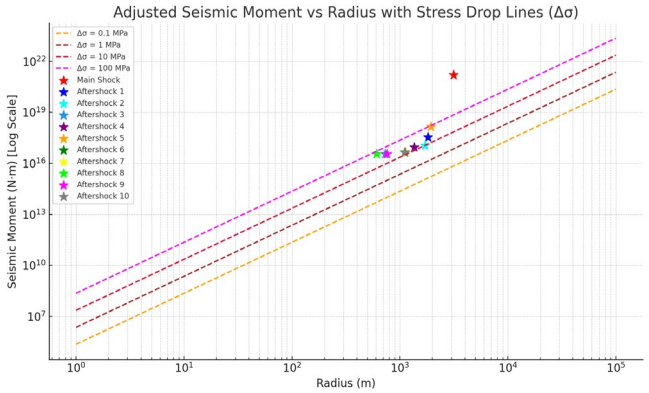

Figure. 11. Log-Log Plot of Seismic Moment vs Fracture Radius with Stress Drop (Δσ) Iso-Lines
Source: The authors.

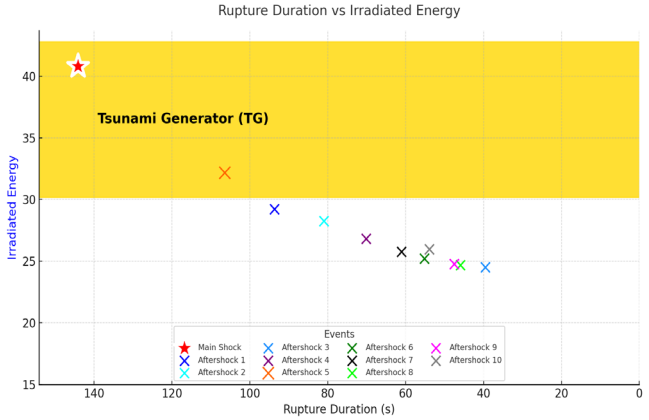

Figure. 12. Relationship between rupture duration and radiated energy for the 2001 Arequipa mainshock and its aftershocks
Source: The authors.

4.4. Maximum radiated energy

The main earthquake radiated 40.80 J of energy, while the aftershocks had values ranging from 21.19 J to 26.29 J, according to analysis using the WT.

Fig. 12 shows the relationship between rupture duration (in seconds) and radiated energy in a seismic context, specifically for a Tsunami Generator (TG). The x-axis measures rupture duration, and the y-axis represents radiated energy (blue). Each point in the graph represents a seismic event, differentiated by colors and shapes. The main earthquake is highlighted with a red star, located in the upper left corner, indicating that it had the longest rupture duration and the highest radiated energy. The other points correspond to aftershocks, labeled in the legend as Aftershock 1, Aftershock 2, etc., with different colors and symbols. It is observed that as the rupture duration decreases, the radiated energy also decreases, suggesting a positive correlation between both variables. The aftershocks exhibit lower energy and shorter rupture durations compared to the main event, which is expected in a seismic sequence.

5. Conclusions

This study applied and compared the Fourier Transform (FFT) and the Wavelet Transform (WT) to analyze the seismic source parameters of the 2001 Arequipa earthquake and ten aftershocks, using SAC and MATLAB. The combined use of both methods enabled a comprehensive characterization of the mainshock and its associated events. The main earthquake (Mw 8.4) exhibited a seismic moment (Mo) of 1.58×10^{21} Nm, significantly higher than the aftershocks, which ranged from 1.12×10^{17} to 1.41×10^{18} N·m, confirming that the mainshock accounted for the majority of energy release along the fault.

The fracture radius for the mainshock was 3.15 km. In comparison, aftershock values ranged from 0.61 km to 1.94 km, indicating that the main rupture encompassed a substantially larger fault area, which triggered the subsequent events.

Stress drop (Δσ) for the main event reached 38.08 MPa, compared to 0.46–3.99 MPa for aftershocks, showing a direct correlation with Mo and supporting rupture mechanics scaling laws.

Radiated energy (MaxEa), estimated through WT, was 40.80 J for the mainshock and between 24.52 J and 32.19 J for aftershocks, highlighting the main event's dominance in energy dissipation across the seismic sequence.

Rupture duration was 146.12 s for the mainshock, versus 40.02–105.98 s for aftershocks, reflecting its greater magnitude and destructive potential.

FFT proved effective in extracting spectral parameters such as Mo, Δσ, and corner frequency, while WT enabled detailed time-frequency analysis, particularly for radiated energy and rupture duration.

Together, FFT and WT offer a complementary framework for seismic source analysis, improving the understanding of fault dynamics and enhancing regional seismic hazard assessment.

Acknowledgments

The authors would like to thank UNSA INVESTIGA (Project PTTMD-42 2023-UNSA) for funding this research work.

References

[1] Gurley, K., and Kareem, A., Applications of wavelet transforms in earthquake, wind, and ocean engineering. Eng Struct. 21(2), pp. 149–167, 1999. DOI: https://doi.org/10.1016/S0141-0296(98)00085-5.

[2] Sinha, S., Routh, P., Anno, P., and Castagna, J., Spectral decomposition of seismic data using continuous wavelet transform. Geophysics, 70(6), art. 27113, 2005. DOI: https://doi.org/10.1190/1.2127113

[3] Rajbhandari, R., Acharya, I.P., and Adhikari, B.R., Application of wavelet transform for seismic wave analysis in Kathmandu. Geoenvironmental Disasters. 6(1), pp. 1–10, 2019. DOI: https://doi.org/10.1186/s40677-019-0134-8.

[4] Hao, J., and Yao, Z., Determination of regional earthquake source parameters in the wavelet domain. Sci China Earth Sci. 55(5), pp. 802–810, 2012. DOI: https://doi.org/10.1007/s11430-011-4341-8.

[5] Longchamp, G., Clares, R, González, J., and Leyva, M., Seismic source parameters of earthquakes located on the eastern fault, in a

sector southeast of Santiago de Cuba province. XI Congr Cubano Geol Simp Riesgo Geol Seismic. 2015.
[6] Cichowicz, A., and Birch, D., Estimation of seismic source parameters. Council for Geoscience, SIM 11-02-01, 2012.
[7] Flórez, C., and Lozano, C., Analysis and processing of signals from seismogenic sources near San José de Cúcuta, Colombia. 2016. DOI: https://doi.org/10.22463/0122820X.569.
[8] Archuleta, R., Cranswick, C., Mueller, C., and Spudich, P., Source parameters of the 1980 Mammoth Lakes, California, earthquake sequence. J. Geophys Res. 87(B6), pp. 4595–4607, 1982. DOI: https://doi.org/10.1029/JB087iB06p04595.
[9] Kanamori, H., and Anderson, L., Theoretical basis of some empirical relations in seismology. Bull Seismol Soc Am. 65(5), pp. 1073–1095, 1975. DOI: https://doi.org/10.1785/BSSA0650051073.
[10] Delgado, M., Determination of seismic source parameters from spectral analysis: applied to the aftershocks of the 2001 Arequipa earthquake. Universidad Nacional de San Agustín, [online]. 2018. Available at: https://repositorio.unsa.edu.pe/handle/UNSA/7045.
[11] Hancco, J., Determination of seismic source parameters through spectral analysis of aftershocks from the January 14, 2018, Lomas earthquake in Arequipa. Universidad Nacional de San Agustín, [online]. 2022. Available at: http://hdl.handle.net/20.500.12773/15610.
[12] Ocola, L., Coseismic subsidence in southern Peru: Mw 8.4 earthquake of June 23, 2001. Adv Geosci. 14, pp. 79–83, 2008. DOI: https://doi.org/10.5194/adgeo-14-79-2008.
[13] Legrand, D., Delouis, B., Dorbath, L., David, C., Campos, J., Marquéz, L., Thompson, J., and Comte, D., Source parameters of the Mw = 6.3 aromatic crustal earthquake of July 24, 2001 (northern Chile) and its aftershock sequence. J South Am Earth Sci. 24(1), pp. 58–68, 2007. DOI: https://doi.org/10.1016/j.jsames.2007.02.004.
[14] Malasavage, N., and Wartman, J., Spatial analysis of the damage distribution from the 2001 southern Peru earthquake. Geotech Earth Eng Soil Dyn IV., 2008. DOI: https://doi.org/10.1061/40975(318)24.
[15] Kuroiwa, J., Sustainable cities, a regional seismic scenario, and the Arequipa, Peru earthquake of June 23, 2001, 2002. DOI: https://doi.org/10.1061/ASCE1527-698820023:4158.
[16] Tavera, H., and Antayhua, Y., Parameters of the Arequipa earthquake of June 23, 2001, and three major aftershocks deduced from spectral analysis of body waves. Inst Geofísico Perú (IGP), Cent Nac Datos Geofís (CNDG), pp. 99–104. 2002.
[17] Fourier, J.B.J., Théorie analytique de la chaleur. Firmin Didot, Paris, 1822.
[18] Unser, M., Fast Gabor-like continuous wavelet transforms with windowed Fourier transforms. IEEE Signal Process Lett. 1(5), pp. 76–79, 1994. DOI: https://doi.org/10.1109/97.294384.
[19] Adhikari, B., Dahal, S., Karki, M., Mishra, R., Dahal, R., Sasmal, S,. and Klausner, V., Application of Wavelet for seismic wave analysis in the Kathmandu Valley after the 2015 Gorkha earthquake, Nepal. Geoenviron Disasters. 7(1), art. 0134-8, 2020. DOI: https://doi.org/10.1186/s40677-019-0134-8.
[20] Daubechies, I., Ten lectures on wavelets. Society for Industrial and Applied Mathematics, 1992. DOI: https://doi.org/10.1137/1.9781611970104.
[21] Chen, J., Wald, D., and Helmberger, D., Source description of the 1999 Hector Mine earthquake, California, Part I: Wavelet domain inversion theory and resolution analysis. Bull Seismol Soc Am. 92(4), pp. 1192–1207, 2002. DOI: https://doi.org/10.1785/0120000916.
[22] Jindal, M., Priya, G., Jothilakshmi, R., Chithra, S., Ramasamy, V., and Kumar, D., Comprehensive study of Fourier and Wavelet transforms: features and applications, 2023. DOI: https://doi.org/10.5281/zenodo.7766175.
[23] Li, H., Yi, T., Gu, M., and Huo, L., Evaluation of earthquake-induced structural damage using wavelet transform. Prog Nat Sci. 19(4), pp. 461–470, 2009. DOI: https://doi.org/10.1016/j.pnsc.2008.09.002.
[24] Chik, Z., Islam, T., Rosyidi, S.A., Sanusi, H., Taha, M.R., and Mustafa, M.M., Comparing the performance of Fourier decomposition and wavelet decomposition for seismic signal analysis. Eur J Sci Res. 32(3), pp. 314–328, 2009.
[25] Helffrich, G., Wookey, J., and Bastow, I., The seismic analysis code: a primer and user's guide. Cambridge University Press, Cambridge, 2013. DOI: https://doi.org/10.1017/CBO9781139547260.
[26] Boudouridis, A., and Zesta, E., Comparison of Fourier and Wavelet techniques in determining geomagnetic field line resonances. J Geophys Res. 112, art. 11922, 2007. DOI: https://doi.org/10.1029/2006JA011922.
[27] Thorsten, B., and Sedl, D., Spectrogram analysis of selected tremor signals using short-time Fourier transform and continuous wavelet transform. Ann Geophys. 42(3), art. 3733, 1999. DOI: https://doi.org/10.4401/ag-3733
[28] Brune, J.B.J., Tectonic stress and spectra of shear waves from earthquakes. J Geophys Res. 75(26), pp. 4997–5009, 1970. DOI: https://doi.org/10.1029/JB075i026p04997.
[29] Hu, X.G., Liu, L., Hinderer, J., Hsu, H., and Sun, H., Analysis of atmospheric pressure effects in the long-period seismic modal band using wavelet filters. Phys Earth Planet Inter. 154(1), pp. 70–84, 2006. DOI: https://doi.org/10.1016/j.pepi.2005.09.003.
[30] Lockwood, O., and Kanamori, H., Wavelet analysis of seismograms from the 2004 Sumatra-Andaman earthquake and its application to tsunami early warning. Geochem Geophys Geosyst. 7(9), art. 1272, 2006. DOI: https://doi.org/10.1029/2006GC001272.
[31] Mamadou, S., Michail, K., Holschneider, M., Scherbaum, F., and Adler, F., Characterization of seismic wave polarization attributes using continuous wavelet transforms. Geophysics. 71(3), art. 94511, 2006. DOI: https://doi.org/10.1190/1.2194511
[32] Hartzell, S., and Liu, P.C., Calculation of earthquake rupture histories using a hybrid global search algorithm. Bull Seismol Soc Am. 86(2), pp. 525–538, 1996.
[33] McNamara, D.E., and Buland, R.P., Ambient noise levels in the continental United States. Bull Seismol Soc Am. 94(4), pp. 1517–1527, 2004.
[34] Iliescu, V., Seismic signal enhancement using time-frequency transforms. Master's thesis. University of Calgary, Calgary, [online]. 2002. Available at: https://ucalgary.scholaris.ca. DOI: https://doi.org/10.11575/PRISM/15751.
[35] Salmon, M.W., Short, S.A., and Kennedy, R.P., Strong motion duration and earthquake magnitude relationships (No. UCRL-CR-117769). Lawrence Livermore National Lab. 1992. DOI: https://doi.org/10.1007/s10009-008-0033-1.
[36] Bessissi, Z., Terbeche, M., and Ghezali, B., Application of wavelets to the analysis of time series of DORIS station coordinates. Comptes Rendus Geosci. 341(6), pp. 446–461, 2009. DOI: https://doi.org/10.1016/j.crte.2009.03.010.

M.K. Paredes-Huanca, received the BSc. Eng. in Geophysical Engineering in May 2025 from the National University of San Agustín in Arequipa, Peru. She holds diplomas in Occupational Health and Safety, Occupational Safety, Health, and Environment from the Ibero-American Institute of Professional Training. From 2020 to 2021, she volunteered at the Latin American Society for Natural Resources Research. In 2021, she completed her professional internship at the Faculty of Geology, Geophysics, and Mining at the National University of San Agustín. From 2022 to 2025, she worked in private companies providing services to the Las Bambas mine, holding positions as Planning Assistant, Operations Supervisor, Safety Supervisor, and Maintenance Planner. She is currently a Safety Supervisor at Myrc Contractors, providing services at the Las Bambas mining unit.
ORCID: 0009-0002-6227-7278

E. Gonzales-Zenteno, holds a PhD. in Water Resources from the Universidad Nacional Agraria La Molina and a Dr. in Industrial Engineering from UNSA. He also holds a MSc. in Mining and Environmental Management from UNI and a BSc. Eng. in Geophysical Engineering from UNSA, where he currently serves as a full professor. He has held key academic leadership positions, including Dean of the Faculty of Geology, Geophysics, and Mining, School Director, and Head of Academic Coordination. He has completed specialized training in geosciences in the United States, France, and Germany, and has participated as a speaker at international conferences across the Americas, Europe, and Asia. He is an active member of professional institutions such as SEG, SME, SOMP, PDAC, IIMP, CIP, and SGP.
ORCID: 0000-0002-9235-9138